

# Iterated Conformal Dynamics and Laplacian Growth

Felipe Barra, Benny Davidovitch and Itamar Procaccia

*Department of Chemical Physics, The Weizmann Institute of Science, Rehovot 76100, Israel*

The method of iterated conformal maps for the study of Diffusion Limited Aggregates (DLA) is generalized to the study of Laplacian Growth Patterns and related processes. We emphasize the fundamental difference between these processes: DLA is grown serially with constant size particles, while Laplacian patterns are grown by advancing each boundary point in parallel, proportionally to the gradient of the Laplacian field. We introduce a 2-parameter family of growth patterns that interpolates between DLA and a discrete version of Laplacian growth. The ultraviolet putative finite-time singularities are regularized here by a minimal tip size, equivalently for all the models in this family. With this we stress that the difference between DLA and Laplacian growth is NOT in the manner of ultraviolet regularization, but rather in their deeply different growth rules. The fractal dimensions of the asymptotic patterns depend continuously on the two parameters of the family, giving rise to a “phase diagram” in which DLA and discretized Laplacian growth are at the extreme ends. In particular we show that the fractal dimension of Laplacian growth patterns is much higher than the fractal dimension of DLA, with the possibility of dimension 2 for the former not excluded.

## I. INTRODUCTION

This paper had been motivated by an apparent consensus on DLA and Laplacian growth Patterns being in the same universality class in terms of their asymptotic fractal dimensions [1]. We present here a theory of these processes in two dimensions which clarifies the differences between these processes, showing in particular that their asymptotic fractal dimensions differ.

Laplacian Growth Patterns are obtained when the boundary  $\Gamma$  of a 2-dimensional domain is grown at a rate proportional to the gradient of a Laplacian field  $P$ . Outside the domain  $\nabla^2 P = 0$ , and each point of  $\Gamma$  is advanced at a rate proportional to  $\nabla P$  [2,3]. In Diffusion Limited Aggregation (DLA) [4] a 2-dimensional cluster is grown by releasing fixed size random walkers from infinity, allowing them to walk around until they hit any particle belonging to the cluster. Since the particles are released one by one and may take arbitrarily long time to hit the cluster, the probability field is stationary and in the complement of the cluster we have again  $\nabla^2 P = 0$ . The boundary condition at infinity is the same for the two problems; in radial geometry as  $r \rightarrow \infty$  the flux is  $\nabla P = \text{const} \times \hat{r}/r$ . Since the probability for a random walker to hit the boundary is again propor-

tional to  $\nabla P$ , one could think that in the asymptotic limit when the size of the particle is much smaller than the radius of the cluster, repeated growth events lead to a growth process which is similar to Laplacian Growth. Of course, the ultraviolet regularizations in the two processes were taken different; in studying Laplacian Growth one usually solves the problem with the boundary condition  $P = \sigma\kappa$  where  $\sigma$  is the surface tension and  $\kappa$  the local curvature of  $\Gamma$  [5]. Without this (or some other) ultraviolet regularization Laplacian Growth reaches a singularity (cusps) in finite time [3]. In DLA the ultraviolet regularization is provided by the finite size of the random walkers. However, many researchers believed [1] that this difference, which for very large clusters controls only the smallest scales of the fractal patterns, were not relevant, expecting the two models to lead to the clusters with the same asymptotic dimensions. While we argue below that the difference in ultraviolet regularization is indeed not crucial, we maintain that the two problems are in two different universality classes.

In this paper we construct a family of growth processes that includes DLA and a discrete version of Laplacian Growth as extreme members, using the same ultraviolet regularization. We thus expose the essential difference between DLA and Laplacian Growth. DLA is grown serially, with the field being updated after each particle growth. On the other hand all boundary points of a Laplacian pattern are advanced in parallel at once (proportional to  $\nabla P$ ). We show that this difference is fundamental to the asymptotic dimension, putting the two problems in different universality classes. An announcement of these results was presented in [6].

To reach these conclusions we formulate a theory of Laplacian Growth patterns in terms of iterated conformal maps. Such a theory was successfully advanced recently for DLA [7–10], providing for an unprecedented analytic control of the properties of DLA [11,12]. By generalizing it to Laplacian Growth patterns we can enjoy similar advantages, allowing us to address delicate points that are beyond the scope of direct numerical simulations and previous analytic attempts.

In Sect. 2 we extend the iterated conformal maps approach to parallel processes of layer-by-layer growth with varying local growth rates. In Sect. 3 we construct a 2-parameter family of parallel growth processes that includes DLA and the discrete Laplacian Growth as special (and distinct) cases. We demonstrate the relevance of the two parameters in determining the asymptotic fractal properties of the resulting patterns. In Sect. 4 we consider our algorithm for Laplacian growth and compare it to the exact dynamics without surface tension.

We study the correspondence between these models for the early dynamics (before the appearance of finite time singularities in the latter). In Sect. 5 we offer concluding remarks.

## II. ITERATED CONFORMAL MAPS FOR PARALLEL GROWTH PROCESSES

The method of iterated conformal maps for DLA was introduced in [7]. Here we present a generalization to parallel growth processes. We are interested in  $\Phi^{(n)}(w)$  which conformally maps the exterior of the unit circle  $e^{i\theta}$  in the mathematical  $w$ -plane onto the complement of the (simply-connected) cluster of  $n$  particles in the physical  $z$ -plane. The unit circle is mapped onto the boundary of the cluster. In what follows we use the fact that the gradient of the Laplacian field  $\nabla P(z(s))$  is

$$\nabla P(z(s)) = \frac{1}{\Phi^{(n)'}(e^{i\theta})}, \quad z(s) = \Phi^{(n)}(e^{i\theta}). \quad (1)$$

Here  $s$  is an arc-length parametrization of the boundary. The map  $\Phi^{(n)}(w)$  is constructed recursively. Suppose that we have already  $\Phi^{(n)}(w)$  which maps to the exterior of a cluster of  $n$  particles in the physical plane and we want to find the map  $\Phi^{(n+p)}(w)$  after  $p$  additional particles were added to its boundary *at once*, each proportional in size to the local value of  $|\nabla P|^{\alpha/2}$ . To grow *one* such particle we employ the elementary map  $\phi_{\lambda,\theta}$  which transforms the unit circle to a circle with a ‘‘bump’’ of linear size  $\sqrt{\lambda}$  around the point  $w = e^{i\theta}$ . In this paper we employ the elementary map [7]

$$\begin{aligned} \phi_{\lambda,0}(w) &= \sqrt{w} \left\{ \frac{(1+\lambda)}{2w} (1+w) \right. \\ &\times \left. \left[ 1+w+w \left( 1 + \frac{1}{w^2} - \frac{2}{w} \frac{1-\lambda}{1+\lambda} \right)^{1/2} \right] - 1 \right\}^{1/2} \end{aligned} \quad (2)$$

$$\phi_{\lambda,\theta}(w) = e^{i\theta} \phi_{\lambda,0}(e^{-i\theta} w), \quad (3)$$

If we update the field after the addition of this single particle, then

$$\Phi^{(n+1)}(w) = \Phi^{(n)}(\phi_{\lambda_{n+1},\theta_{n+1}}(w)), \quad (4)$$

where  $\Phi^{(n)}(e^{i\theta_{n+1}})$  is the point on which the  $(n+1)$ -th particle is grown and  $\sqrt{\lambda_n}$  is the size of the grown particle divided by the Jacobian of the map  $\Phi^{(n)'}(e^{i\theta_{n+1}})$  at that point.

The map  $\Phi^{(n)}(w)$  adds on a new semi-circular bump to the image of the unit circle under  $\Phi^{(n-1)}(w)$ . The bumps in the  $z$ -plane simulate the accreted particles in the physical space formulation of the growth process. For the height of the bump to be proportional to  $|\nabla P(z(s))|^{\alpha/2}$  we need to choose its area proportional to  $|\Phi^{(n-1)'}(e^{i\theta_n})|^{-\alpha}$  (see Eq. (1)), or

$$\lambda_n = \frac{\lambda_0}{|\Phi^{(n-1)'}(e^{i\theta_n})|^{\alpha+2}}. \quad (5)$$

With  $\alpha = 0$  these rules produce a DLA cluster. Next, to grow  $p$  (non-overlapping) particles in parallel, we accrete them without updating the conformal map. In other words, to add a new layer of  $p$  particles when the cluster contains  $m$  particles, we need to choose  $p$  angles on the unit circle  $\{\tilde{\theta}_{m+k}\}_{k=1}^p$ . At these angles we grow bumps which in the physical space are proportional in size to the gradient of the field around the  $m$ -particle cluster:

$$\lambda_{m+k} = \frac{\lambda_0}{|\Phi^{(m)'}(e^{i\tilde{\theta}_{m+k}})|^{\alpha+2}}, \quad k = 1, 2, \dots, p. \quad (6)$$

After the  $p$  particles were added, the conformal map and the field should be updated. In updating, we will use  $p$  compositions of the elementary map  $\phi_{\lambda,\theta}(w)$ . Of course, every composition effects a reparametrization of the unit circle, which has to be taken into account. To do this, we define a series  $\{\theta_{m+k}\}_{k=1}^p$  according to

$$\Phi^{(m)}(e^{i\tilde{\theta}_{m+k}}) \equiv \Phi^{(m+k-1)}(e^{i\theta_{m+k}}). \quad (7)$$

Next we define the conformal map used in the next layer growth according to

$$\Phi^{(m+p)}(\omega) \equiv \Phi^{(m)} \circ \phi_{\theta_{m+1},\lambda_{m+1}} \circ \dots \circ \phi_{\theta_{m+p},\lambda_{m+p}}(\omega). \quad (8)$$

In this way we achieve the growth at the images under  $\Phi^{(m)}$  of the points  $\{\tilde{\theta}_{m+k}\}_{k=1}^p$ . To compute the  $\theta$  series from a given  $\tilde{\theta}$  series we use Eq.(8) to rewrite Eq.(7) in the form

$$e^{i\theta_{m+k}} = \phi_{\theta_{m+k-1},\lambda_{m+k-1}}^{-1} \circ \dots \circ \phi_{\theta_{m+1},\lambda_{m+1}}^{-1}(e^{i\tilde{\theta}_{m+k}}) \quad (9)$$

The inverse map  $\phi_{\theta,\lambda}^{-1}$  is given by  $\phi_{\theta,\lambda}^{-1}(\omega) = e^{i\theta} \phi_{0,\lambda}^{-1}(e^{-i\theta} \omega)$  with

$$\phi_{0,\lambda}^{-1} = \frac{\lambda\omega^2 \pm \sqrt{\lambda^2\omega^4 - \omega^2[1 - (1+\lambda)\omega^2][\omega^2 - (1+\lambda)]}}{1 - (1+\lambda)\omega^2}, \quad (10)$$

where the positive root is taken for  $\text{Re } \omega > 0$  and the negative root for  $\text{Re } \omega < 0$ . We stress that if we had taken  $\theta_n = \tilde{\theta}_n$ , neglecting the effects of reparametrization, we would find abnormally small bumps on the tips. The reparametrization tends to move arcs that have to be mapped to fjords to regions that are mapped to tips. Then bumps that were supposed to grow in fjords where their size were normal would be pushed to tips where their size becomes extremely small; small bumps would appear where they do not belong.

In Fig. 1 we present a schematic diagram of the parallel growth described above.

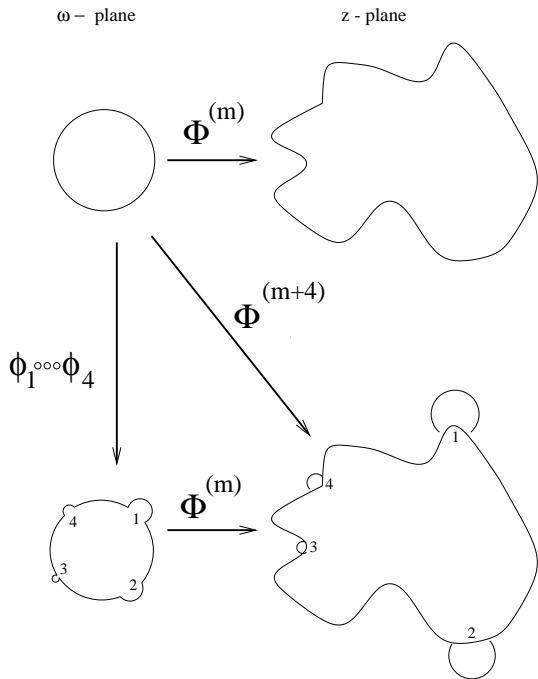


FIG. 1. A schematic diagram of parallel growth with four particles. The points 1-4 in the mathematical ( $\omega$ ) plane stand for  $\tilde{\theta}_1 \dots \tilde{\theta}_4$ , and are mapped under  $\Phi^{(m)}$  to the appropriate images in the physical ( $z$ ) plane. The sizes of the bumps were chosen to simulate  $\alpha > 0$ .

It is important to notice that on the face of it the conformal map (8) appears very similar to the one obtained in DLA, [7,8]. But this is deceptive. Here we summarize the three major differences between DLA and the new growth models:

- The distribution  $\{\tilde{\theta}\}_{i=1}^n$  (which is chosen uniform in DLA and related growth models, [9]) is transformed to a nonuniform (and maybe even singular) distribution of the angles  $\{\theta\}_{i=1}^n$ .
- The field by which we calculate  $\lambda_n$  (i.e. the derivative of the conformal map) is not updated after each step, but only after growing a number of particles, and in the limit a whole layer.
- the parameter  $\alpha$  in Eq. (6) can be taken to be different than 0 (which is the value used to grow DLA clusters). In particular with  $\alpha = 2$  the size of the bump is proportional to the gradient of the local field, as is appropriate for Laplacian Growth.

Note that our algorithm is not purely parallel, as the composition in Eq.(8) indicates. The parallel aspect is in using the same *field* to compute the values of  $\lambda_n$  in Eq. (6) and choosing a uniform distribution of  $\{\tilde{\theta}\}_{i=1}^n$  instead of  $\{\theta\}_{i=1}^n$ . Note that here and below when we say a “uniform distribution” we mean that the series was created without any preference for any region of the unit circle. It very well may be that after avoiding overlaps the resulting distribution may be unevenly represented

over the unit circle. Anyway we make use of an ordered series of compositions of the basic map  $\phi$  to construct one layer. In the next section we will show that the serial aspect of the layer growth is not important in terms of the asymptotic fractal dimension of the clusters. In other words, the order of placing the bumps is not relevant as long as the same field is used as in Eq. (6).

The details of the algorithm, including how to choose the series  $\{\tilde{\theta}_{m+k}\}_{k=1}^p$  to avoid overlaps are presented in Appendix A.

### III. TWO-PARAMETER FAMILY OF GROWTH PROCESSES

Evidently, a discretized Laplacian Growth calls for choosing the series  $\{\tilde{\theta}_{m+k}\}_{k=1}^p$  such as to have full coverage of the unit circle (implying the same for the boundary  $\Gamma$ ). On the other hand DLA calls for growing a single particle before updating the field. Since it was shown that in DLA growth  $\lambda_n$  decreases on the average when  $n$  increases, in the limit of large clusters DLA is consistent with vanishingly small coverage of the unit circle. To interpolate between these two cases we introduce a parameter that serves to distinguish one growth model from the other, giving us a 1-parameter control (the other parameter is  $\alpha$ ). This parameter is the *degree of coverage*. Since the area covered by the pre-image of the  $n$ -th particle on the unit circle is approximately  $2\sqrt{\lambda_n}$ , we introduce the parameter

$$\mathcal{C} = \frac{1}{\pi} \sum_{k=1}^p \sqrt{\lambda_{m+k}}. \quad (11)$$

(In the Appendix A we show how to measure the coverage exactly). Since this is the fraction of the unit circle which is covered in each layer, the limit of Laplacian Growth is obtained with  $\mathcal{C} = 1$ . DLA is asymptotically consistent with  $\mathcal{C} = 0$ . Of course, the two models differ also in the size of the growing bumps, with DLA having fixed size particles, ( $\alpha = 0$  in Eq.(5)), and Laplacian Growth having particles proportional to  $\nabla P$  ( $\alpha = 2$  in Eq.(6)). Together with  $\mathcal{C}$  we have a two parameter control on the parallel growth dynamics, with DLA and Laplacian Growth occupying two corners of the  $\alpha, \mathcal{C}$  plane, at the points (0,0) and (2,1) respectively.

Needless to say, with our partially serial growth within the layer, we introduced an extra freedom which is the *order* of placement of the bumps on the unit circle. In order for the model to have a physical meaning (i.e. to simulate true Laplacian growth), it must not depend on the specific itinerary of  $\{\tilde{\theta}_i\}_{i=m+1}^{m+p}$  used to cover the unit circle as long as it is uniformly distributed on the unit circle. We will show first that this extra freedom has no consequence with regards to the asymptotic dimension of the resulting cluster. For fixed  $\alpha$  the dimension depends only on the value of  $\mathcal{C}$ . To demonstrate this, we will

consider various itineraries to achieve a uniform coverage  $\mathcal{C}$ .

One way is to construct the “golden mean trajectory”

$$\tilde{\theta}_{m+k+1} = \tilde{\theta}_{m+k} + 2\pi\rho$$

where  $\rho = (\sqrt{5} - 1)/2$ . At each step we check whether the newly grown bump may overlap a previous one in the layer. If it does, this growth step is skipped and the orbit continues until a fraction  $\mathcal{C}$  is covered. The first bump of the next layer is grown at a random position in order to eliminate correlations induced by the arbitrary itinerary chosen to grow the previous layer. Another method is random choices of  $\tilde{\theta}_{m+k}$  with the same rule of skipping overlaps. A third method is what was termed in [9] the “period doubling” itinerary

$$\tilde{\theta}_0 = 0, \quad \tilde{\theta}_{2^n+k} = \tilde{\theta}_k + \frac{2\pi}{2^{n+1}}, \quad 0 \leq k < 2^n, n \geq 0 \quad (12)$$

In all these methods we cannot reach  $\mathcal{C} = 1$ , since there are gaps left between the bumps. These are excluded from further growth in the present layer since their sizes are smaller than the corresponding value of  $\sqrt{\lambda_n}$  as calculated in the middle of the gap. We can estimate the maximal value of  $\mathcal{C}$  to be of the order of 0.65. Nevertheless, to be an acceptable model of parallel growth the fractal dimension of the resulting cluster should be invariant to the itinerary. This invariance is demonstrated below. In the next section we treat the case  $\mathcal{C} = 1$  by constructing an ordered series with extra care. In the rest of this section we demonstrate the irrelevance of the itinerary.

With the present technique it is straightforward to determine the dimension of the resulting cluster. The conformal map  $\Phi^{(n)}(\omega)$  admits a Laurent expansion

$$\Phi^{(n)}(\omega) = F_1^{(n)}\omega + F_0^{(n)} + \frac{F_{-1}^{(n)}}{\omega} + \dots \quad (13)$$

The coefficient of the linear term is the Laplace radius, and was shown to scale like [7,8]

$$F_1^{(n)} \sim S^{1/D}, \quad (14)$$

where  $S$  is the area of the cluster,

$$S = \sum_{j=1}^n \lambda_j |\Phi^{(j-1)'}(e^{i\theta_j})|^2. \quad (15)$$

Note that for  $\alpha = 0$  this and equation (5) imply that  $S = n\lambda_0$ . Indeed for  $\alpha = 0$  this estimate had been carefully analyzed and substantiated (up to a factor) in [10]. On the other hand  $F_1^{(n)}$  is given analytically by

$$F_1^{(n)} = \prod_{k=1}^n \sqrt{1 + \lambda_k}, \quad (16)$$

and therefore can be determined very accurately.

In order to achieve comparable growth rates for different layers we inflated  $\lambda_0$  in Eq.(6) according to  $\lambda_0 \rightarrow m\lambda_0$  in the layer composed of  $p$  particles  $\{m+k\}_{k=1}^p$ . The exact form of inflation is not important; we introduce it simply to oppose the slowing down due to the decrease of  $\langle \lambda_n \rangle$  with  $n$ . In Fig. 2 we show  $F_1$  of clusters grown by choosing the three different itineraries discussed above to produce the layers and for two values of  $\mathcal{C}$ . We note that the curves superpose for the 3 different clusters with the same value of  $\mathcal{C}$ ; for different values of  $\mathcal{C}$  a different behavior of  $F_1$  is manifested.

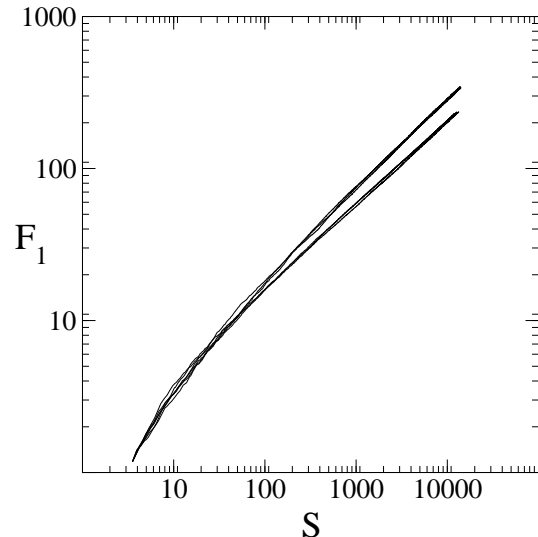


FIG. 2. Log-log plots of  $F_1$  vs.  $S$  of six individual clusters with  $\alpha = 2$ , using 3 different itineraries for layer construction, with two values of  $\mathcal{C}$ .  $\mathcal{C} = 0.3$  (upper group) and  $\mathcal{C} = 0.5$  (lower group). Here we use the golden-mean, random and the period doubling itineraries (see Ref.[9]).

We conclude that the dimension (determined by the asymptotic behavior of  $F_1$  vs.  $S$ ) does not depend on the itinerary used to form the layers but on  $\mathcal{C}$  only. To understand this further we note that changing  $\mathcal{C}$  for a fixed value of  $\alpha$  is equivalent to changing the growth probability. For example, if we perform growth with  $\mathcal{C} = 1$  and  $\alpha = 0$  we generate compact clusters, since we grow fixed size particles with a uniform measure.  $\mathcal{C} = 0$  and  $\alpha = 0$  is DLA even if we choose a fixed, or even a growing number of particles in each layer, as long as  $\mathcal{C} \rightarrow 0$  asymptotically. In Fig.3 we demonstrate this fact by simulating growth with 1 particle in each layer (DLA), and growth with random addition of particles to each layer until the first overlap. In both cases  $\mathcal{C} = 0$ , as the number of particles in each layer grows slower than the available number of sites, and see Sect. 5 for a proof of this statement. Accordingly the dimension is invariant, despite the fact that the number of particles in each layer increases to infinity with the cluster size.

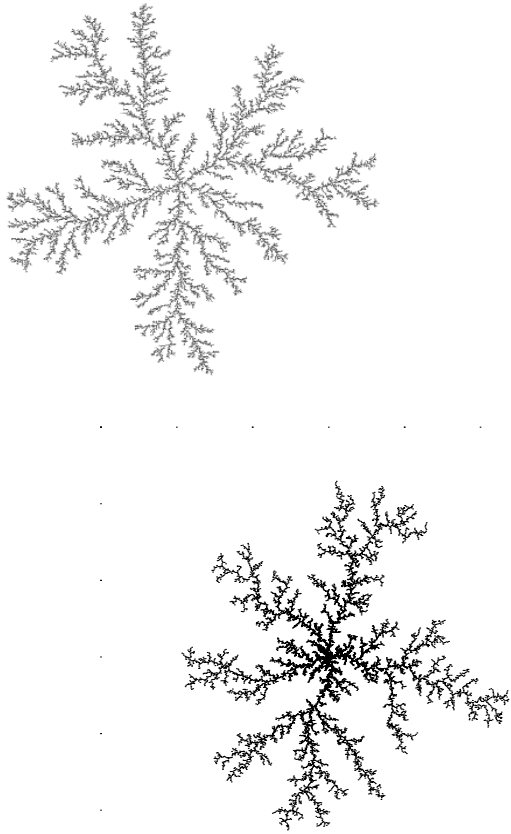


FIG. 3. (a) Regularly grown DLA (1 particle in a layer). (b) Cluster grown by randomly attaching bumps in each layer until the first overlap. Both clusters contain 10 000 particles

In Fig.4 we show three fractal patterns grown with three different values of  $\mathcal{C} > 0$ . We draw the reader's attention to the fact that drawing cluster like the one in panel c is not entirely trivial. Simply mapping the unit circle will not work since many of the fjords will be lost. In fact, in appendix C we develop a reliable and effective method to produce the border of the fractal cluster.

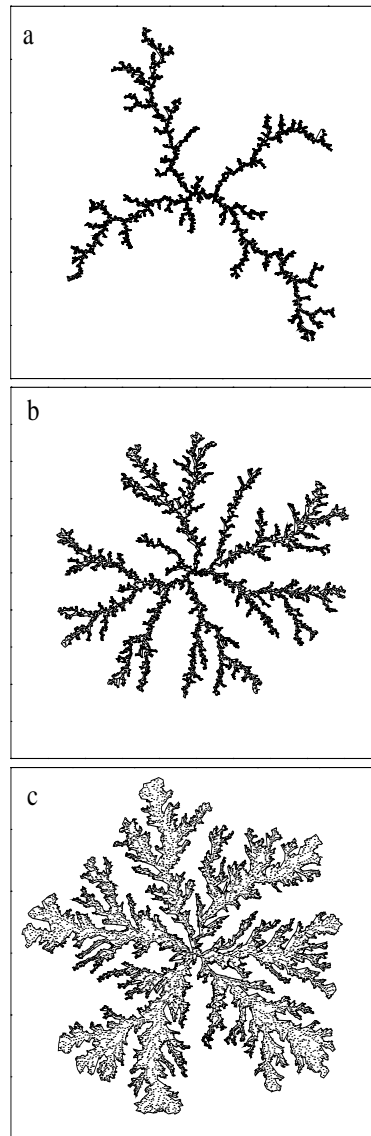


FIG. 4. Patterns grown with  $\alpha = 2$  and 3 different values of  $\mathcal{C}$  by using the golden-mean itinerary: a)  $\mathcal{C} = 0.1$ , b)  $\mathcal{C} = 0.3$ , c)  $\mathcal{C} = 0.5$ .

Even a cursory observation of these patterns should convince the reader that the dimension of these patterns grows upon increasing  $\mathcal{C}$ . For a quantitative determination of the dimension we averaged  $F_1$  of clusters produced by the golden mean itinerary, each with another random initial angle in each layer. Plots of the averages  $\langle F_1 \rangle$  for 3 values of  $\mathcal{C}$  are presented in Fig. 5.

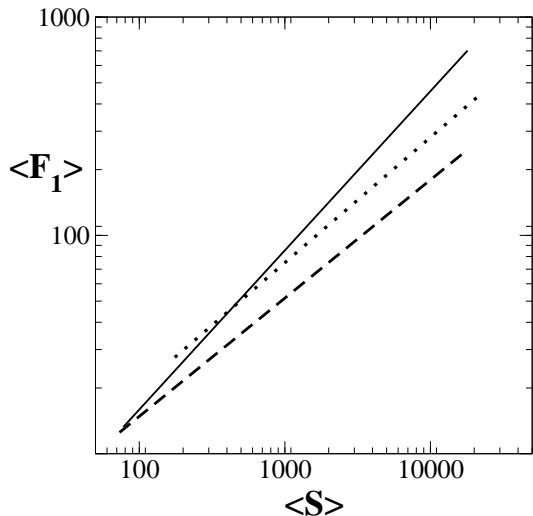


FIG. 5. Linear regressions of log-log plots of  $\langle F_1 \rangle$  vs.  $S$  for  $\alpha = 2$  and 3 values of  $\mathcal{C}$ : 0.1 (solid line), 0.3 (dotted) and 0.6 (dashed). The slopes of the curves imply dimensions  $D=1.37$ ,  $D=1.75$  and  $D=1.85$  respectively. The averages are taken over 20 clusters.

We conclude that the dimension of the growth pattern increases monotonically with  $\mathcal{C}$ , with  $D \approx 1.85$  when  $\mathcal{C} = 0.6$ .

In Fig.6 we present the  $\alpha, \mathcal{C}$  “phase diagram” which results from calculations for a variety of values of  $\mathcal{C}$  and  $\alpha$ .

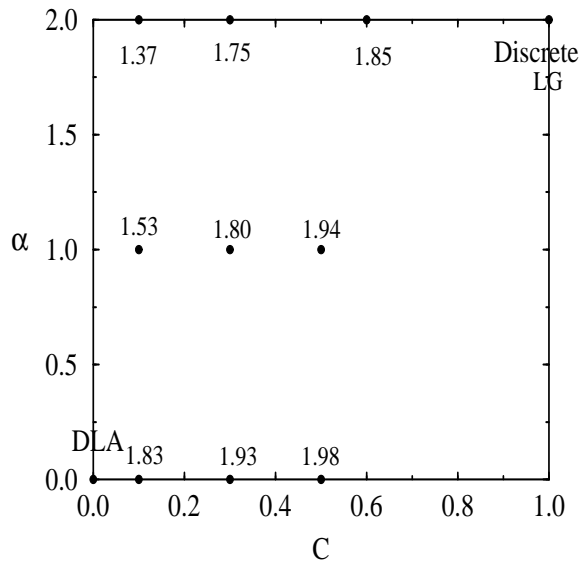


FIG. 6. “Phase diagram” in which the fractal dimension  $D$  is displayed for selected values of the parameters  $\mathcal{C}$  and  $\alpha$ .

The conclusion from these calculations is that the fractal dimension of the clusters depends continuously on the parameters, growing monotonically upon decreasing  $\alpha$  or increasing  $\mathcal{C}$ . It is quite obvious why increasing  $\mathcal{C}$  should increase the dimension, we simply force particles

into the fjords not allowing them to hit the tips only as is highly probable. Also decreasing  $\alpha$  to  $\alpha = 0$  increases the dimension, since we grow equal size particles into the fjords, whereas increasing  $\alpha$  reduces the size of particles added to fjords and increases the size of particles that accrete onto tips. In particular it is obvious that DLA and our discretized Laplacian Growth cannot have the same dimensions, putting them in different universality classes. In particular the dimension  $D = 1.85$  obtained for  $\alpha = 2$  and  $\mathcal{C} = 0.6$  is a lower bound for the dimension of Laplacian Growth patterns. This is because the dimension increase with  $\mathcal{C}$  and  $\mathcal{C} = 1$  for Laplacian Growth patterns. In the next section we present evidence, by reconsidering  $\mathcal{C} = 1$ , that the crucial difference between DLA and Laplacian Growth is not in the discretization or in the ultraviolet regularization, but rather stems from the different values of  $\alpha$  and  $\mathcal{C}$ .

Before turning to models with  $\mathcal{C} = 1$  we note in passing that the present family of models warrants further study on its own right, independently of the relation between DLA and Laplacian Growth. The wealth of growth structures seen in electro-deposition, dielectric breakdown models, and bacterial colony growth [13] may very well justify 2-parameter families of models. The present one is not less physical than any other that had been studied so far in the literature, but it enjoys the benefit of easily obtained conformal formulation.

#### IV. DISCRETE VERSUS CONTINUOUS LAPLACIAN GROWTH

Continuous Laplacian growth without surface tension has been studied using dynamics of conformal maps in [2,3]. The dynamical equation for the conformal map reads

$$\text{Re}\{\omega \overline{\Phi'(\omega, t)} \Phi_t(\omega, t)\} = 1. \quad (17)$$

As is well known, the solutions of this equation generate finite time singularities from smooth initial data. The simplest example is the initial condition

$$\Phi(\omega, 0) = F_1(0)\omega + \frac{F_{-2}(0)}{\omega^2}. \quad (18)$$

The number of Laurent coefficients is preserved by Eq.(17) with

$$\frac{F_1^2(t)}{F_{-2}(t)} = \text{const}. \quad (19)$$

The finite time singularity is seen from the analytic result (writing  $F_j \equiv F_j(0)$ )

$$\begin{aligned} F_1(t) &= \frac{F_1}{2F_{-2}} \sqrt{F_1^2 - \sqrt{[F_1^2 - 4F_{-2}^2]^2 - 8tF_{-2}^2}} \\ F_{-2}(t) &= \frac{1}{4F_{-2}} [F_1^2 - \sqrt{[F_1^2 - 4F_{-2}^2]^2 - 8tF_{-2}^2}]. \end{aligned} \quad (20)$$

At  $t \rightarrow t_c = [F_1^2 - 4F_{-2}^2]^2 / 8F_{-2}^2$ ,  $F_1(t)/F_{-2}(t) \rightarrow 2$  and a cusp is developed at the images of  $1$ ,  $\exp(\frac{2\pi i}{3})$ , and  $\exp(\frac{4\pi i}{3})$ , see Fig.7 . This simple example motivated attempts to understand the role of surface tension as an ultraviolet regularization, see [14]. We will use this result to study further the correspondence between our discretized Laplacian growth and the continuous counterpart, and to solidify the fundamental difference between the latter process and DLA.

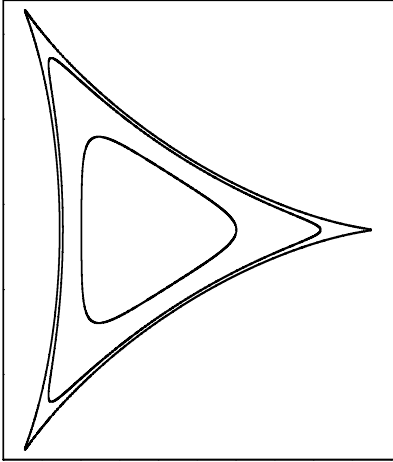


FIG. 7. Evolution of cusps starting from smooth initial conditions, with  $F_1(0) = 1$ ,  $F_{-2}(0) = 0.24$ . Curves are shown at initial time  $t = 0$ , an intermediate time and at the critical time  $t = t_c$ .

As explained in Sec.3, reaching  $\mathcal{C} = 1$  is impossible with any of the itineraries discussed above. We can achieve this limit by growing in an ordered fashion, adding bumps in a controlled manner, precisely such as to glue one branch cut to its neighboring one. How to do this while imposing the appropriate symmetries is explained in detail in Appendices A and B. We discover that the growth patterns constructed in this way tend to fractalize rapidly due to the existence of the branch cuts, in agreement with our statement above that the result of our process is a faithful lower bound to the dimension of continuous Laplacian Growth. An example of the patterns grown by our discretized process from the initial conditions (18) is shown in Fig.8.

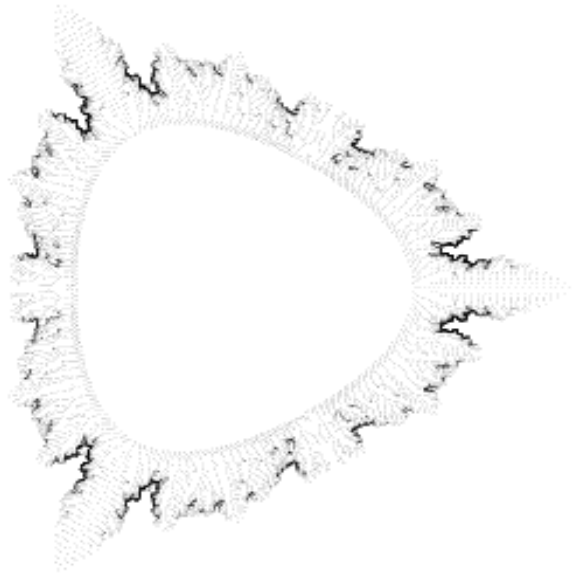


FIG. 8. Cluster grown with  $\mathcal{C} = 1$  starting from the same initial conditions as in Fig.7. Notice that the branch cuts lead to spurious fractalization of the smooth envelope.

The idea of this section is to isolate the effects of the parameter  $\mathcal{C}$  and  $\alpha$  from effects of discretization and ultraviolet regularization. To this end we eliminate the instabilities caused by the bumpiness by keeping track of the two Laurent coefficients  $F_1$  and  $F_{-2}$ . We start with the initial conditions  $F_1(0)\omega + F_{-2}(0)/\omega^2$ . Every layer is then grown by our algorithm with a chosen values of  $\mathcal{C}$  and  $\alpha$ , computing the new values of  $F_1$  and  $F_{-2}$ , using the analytic formulae presented in [8]. Discarding all the other Laurent coefficients we have an updated conformal map in the form  $F_1^{(n)}\omega + F_{-2}^{(n)}/\omega^2$ .

We find the results of this exercise quite revealing. In Fig.9 we show the computed values of  $F_1^{(n)}$  and  $F_{-2}^{(n)}$  and the ratio (19) for  $\mathcal{C} = 1$  and  $\alpha = 2$ , together with other values of these parameters. *For  $\mathcal{C} = 1$  and  $\alpha = 2$  the solution approximates rather closely the exact results up to the creation of the finite time singularity*, with large deviations appearing only when the tip radius of curvature is of the order of  $\lambda_0$ . The degree of approximation improves when  $\lambda_0$  is reduced. On the other hand, the same procedure with other values of  $\mathcal{C}$  or  $\alpha$  deviates from the exact results immediately, with the degree of deviation being monotonic in the difference in values of  $\mathcal{C}$  from unity and of  $\alpha$  from 2.

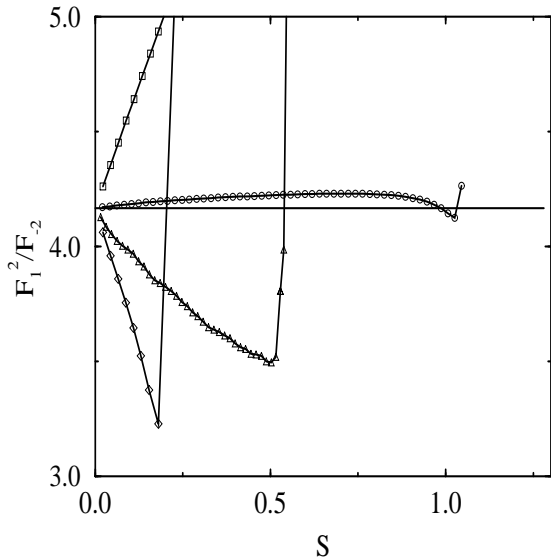


FIG. 9.  $F_1^2/F_{-2}$  as a function of  $S$  for the smooth process described in the text, and for the following values of  $\mathcal{C}$  and  $\alpha$ : circles,  $\mathcal{C} = 1$  and  $\alpha = 2$ ; squares,  $\mathcal{C} = 1$  and  $\alpha = 0$ ; diamonds,  $\mathcal{C} = 1$  and  $\alpha = 4$ ; triangles,  $\mathcal{C} = 0.5$  and  $\alpha = 2$ . The solid line represents the initial conditions which remain constant, Eq.(19).

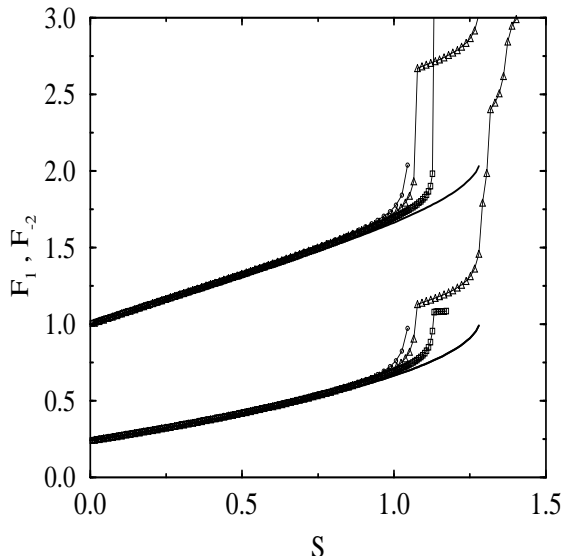


FIG. 10.  $F_1$  and  $F_{-2}$  for the smooth growth process described in the text with  $\mathcal{C} = 1$  and three different values of  $\lambda_0$ . Circles  $\lambda_0 = 10^{-4}$ , triangles  $\lambda_0 = 5 * 10^{-5}$  and squares  $\lambda_0 = 10^{-5}$ . The solid line results from solving (17) with the same initial conditions.

It is not uninteresting to note the similarity between the effect of the finite size particles and surface tension. This is demonstrated in Fig.10. The deviation from the analytic solution depends on  $\lambda_0$ . The smaller the latter

is, the deeper we go into the cusp formation, and the closer we get to the singularity time  $t_c$ . We estimate the time of deviation by comparing the radius of curvature to the physical size of our particle at the tip. This means that at the tip

$$\frac{\lambda_0}{|\Phi'(\text{tip})|^2} \approx \frac{1}{\kappa^2}, \quad (21)$$

where  $\kappa$  is the curvature at the tip. The RHS vanishes when  $t \rightarrow t_c$ , inhibited here by the value of  $\lambda_0$ . The time of deviation is therefore when  $\lambda_0 = |\Phi'(\text{tip})|^2(t)/\kappa^2(t)$ . We can compute the quantities involved analytically:

$$\Phi'(\text{tip}) = F_1 - 2F_{-2}, \quad (22)$$

$$\kappa = \frac{F_1 + 4F_{-2}}{(F_1 - 2F_{-2})^2}. \quad (23)$$

Accordingly we can estimate the time of deviation and compare it with the numerics. The agreement is excellent.

At this point it is worthwhile to reexamine the consensus formed in favor of DLA and Laplacian Growth being in the same universality class. Superficially one could say that in DLA the update of the harmonic measure after each particle is not so crucial, since the effect of such an update is relatively *local* [15]. Thus it may just work that a full layer of particles would be added to the cluster before major interaction between different growth events takes place. However this view is completely wrong. An incoming random walker lands on top of a previously attached one *very often*. To see this, consider how many angles  $\{\theta_j\}$  can be chosen *randomly* on the unit circle before the first overlap between bumps of linear sizes  $\epsilon_j = \sqrt{\lambda_n}(e^{i\theta_j})$ . To get the order of magnitude take  $\epsilon_j = \epsilon = \langle \sqrt{\lambda_n} \rangle$ . The average number of times that we can choose randomly an angle before the first overlap is  $\mathcal{N}(\epsilon) \sim \frac{1}{\sqrt{\epsilon}}$ . The Length of the unit circle that is covered at that time by the already chosen bumps is  $\mathcal{L}(\epsilon) = \epsilon \mathcal{N}(\epsilon) \sim \sqrt{\epsilon}$ . It was shown in [8] that for DLA  $\langle \lambda_n \rangle \sim \frac{1}{n}$ , so that  $\epsilon \sim \frac{1}{\sqrt{n}}$ , implying  $\mathcal{N}(n) \sim n^{1/4}$ . Notice that this result means in particular that for a DLA cluster of 1 million particles only less than 50 random walkers can be attached before two of them will arrive at the same site! Moreover,  $\mathcal{L}(n) \sim \frac{1}{n^{1/4}} \rightarrow 0$  for  $n \rightarrow \infty$ , which means that as the DLA cluster grows, our coverage parameter  $\mathcal{C}$  goes to zero, rather than to unity where Laplacian Growth is. Taking spatial fluctuations of  $\lambda_n$  into account may change the exact exponents but not the qualitative result. This argument clarifies the profound difference between growing a whole layer simultaneously and particle-by-particle. Note however that DLA is NOT the  $\mathcal{C} \rightarrow 0$  limit of our 1-parameter family because  $\alpha = 0$  in Eq. (5) for DLA and  $\alpha = 2$  in Eq. (6) for Laplacian patterns. We will now show that if we eliminate the basic instability that stems from particles landing on each other *then* DLA and Laplacian growth coincide. To do so we start again with the initial conditions  $F_1(0)\omega + F_{-2}(0)/\omega^2$ , grow *one particle* with the



DLA rules, compute the new value of  $F_1$  and  $F_{-2}$ , and use the new map  $F_1^{(n)}\omega + F_{-2}^{(n)}/\omega^2$  as “initial conditions” for an additional particle growth. The results of this process are shown in Fig.11, which is now indistinguishable from Laplacian growth with  $\mathcal{C} = 1$ . In fact, when the instability produced by particles landing one on top of the other is eliminated, the choice of the bumps according to the harmonic measure simulates the growth of a layer, as was expected by many researchers. The presence of the instability which is intimately linked to the DLA growth rules makes it fundamentally different from the parallel layer growth of Laplacian dynamics. We believe that with this discussion we offered a conclusive evidence for the fundamental difference between DLA and Laplacian Growth.

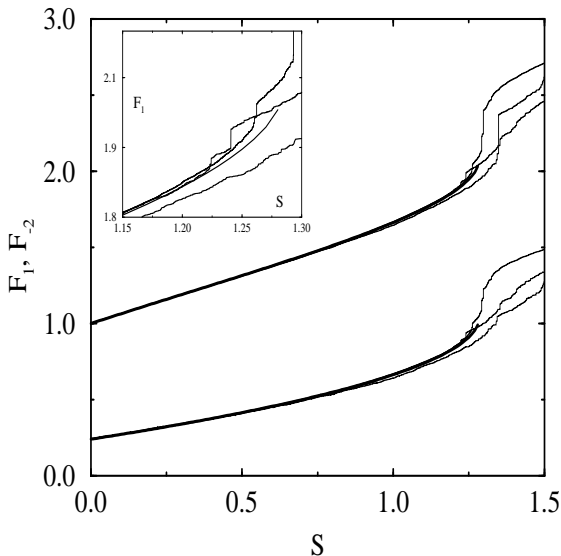


FIG. 11. Growth Patterns as in Fig.10, starting from the same initial conditions but growing particle by particle according to the DLA rules, preserving only  $F_1$  and  $F_{-2}$ . The inset shows a zoom of  $F_1$  close to the time singularity.

## V. CONCLUSIONS AND REMARKS

We have introduced a 2-parameter family of growth patterns with the aim of clearly separating DLA from Laplacian Growth. We explained how to grow in parallel, taking care of the delicate issue of reparametrization. For the latter issue we needed the inverse map as explained in Sect. 2. The tools developed to study and control the reparametrization are further employed to develop symmetry preserving growth algorithms (Appendix B) and efficient methods to construct the interface of fractal clusters (Appendix C). We argued that the parameters  $\mathcal{C}$  and  $\alpha$  are relevant for the asymptotic dynamics, whether the order of placing the bumps is not. The dimensions of the resulting growth patterns were shown to depend continuously on the two parameters. Besides providing

us with a new model which is interesting by itself, we could reach the following main conclusions:

- DLA and Laplacian Growth are not in the same universality class.
- The dimension of Laplacian Growth patterns had been bounded from below by 1.85. We do not have a sharp estimate of this dimension, and cannot exclude  $D = 2$ .
- The difference between DLA and Laplacian Growth models is not in the ultraviolet regularization. We explained that the deep difference is between the serial and parallel growth events, leading to increased tendency to form spikes in DLA.

In future work it may be worthwhile to attempt to find a sharper estimate of the dimension of Laplacian Growth patterns. It seems also worthwhile to study the connection of the present model to models with noise-reduction, and to further understand how to interpret the rich phenomenology of electro-deposition and bacterial colony growth.

## ACKNOWLEDGMENTS

It is a pleasure to thank Mitchell J. Feigenbaum, H. George E. Hentschel and Anders Levermann for invaluable discussions and suggestions. This work has been supported in part by the European Commission under the TMR program and the Naftali and Anna Backenroth-Bronicki Fund for Research in Chaos and Complexity.

## APPENDIX A: DETAILS OF THE ALGORITHM

This appendix consists of three parts. In the first we explain how the absence of overlaps between grown particles can be defined in terms of the conformal map. The second part of this appendix is dedicated to a detailed description of the algorithm that was introduced in Sect. 2. In the last Subsection we explain the algorithm used to achieve  $\mathcal{C} = 1$  at each layer.

### 1. overlaps in terms of iterated conformal maps

Suppose that the first particle in a new layer is the  $(m + 1)$ -th particle in the growth process, and that there are no overlaps between the first  $k$  particles grown in this layer.

In order to express this in terms of the iterated conformal map formalism, let us make the following definitions:

- $\tilde{\omega}_n^{R,L}$  are the two branch points of the map  $\phi_{\tilde{\theta}_n, \lambda_n}$ , denoted as “right” and “left” respectively.

- $\omega_n^{R,L}$  are the two branch points of the map  $\phi_{\theta_n, \lambda_n}$ , (which we denote in the sequel as  $\phi_n$  for brevity).

Let us further denote:

$$e^{i\beta_n^{R,L}} \equiv \phi_n(\omega_n^{R,L}). \quad (\text{A1})$$

Note that  $|\beta_n^R - \beta_n^L|/(2\pi)$  is the fraction of the unit circle covered by the particle.

The angles  $\beta_n^{R,L}$  and  $\arg[\tilde{\omega}_n^{R,L}]$  are connected to each other in a similar manner to the way  $\theta_n$  is connected to  $\tilde{\theta}_n$  (9):

$$\begin{aligned} e^{i\beta_n^R} &= \phi_{n-1}^{-1} \circ \dots \circ \phi_{m+1}^{-1}(\tilde{\omega}_n^R) \\ e^{i\beta_n^L} &= \phi_{n-1}^{-1} \circ \dots \circ \phi_{m+1}^{-1}(\tilde{\omega}_n^L). \end{aligned} \quad (\text{A2})$$

Notice that the inverse function  $\phi_n^{-1}$  is analytic on the unit circle only outside the arc  $[\beta_n^R, \beta_n^L]$ .

If the  $k$ -th particle does not overlap any of the previously grown particles of the layer, then the three points  $\Phi^{(m+k)}(\omega_{m+k}^R)$ ,  $\Phi^{(m+k)}(\omega_{m+k}^L)$ , and  $\Phi^{(m+k-1)}(e^{i\theta_{m+k}})$  are all in the image of the unit circle under  $\Phi^{(m)}$ . In other words, Eqs. (9) and (A2) (for  $n = m+k$ ) are solvable.

Since  $\phi_n^{-1}$  is analytic on the unit circle only outside the arc  $[\beta_n^L, \beta_n^R]$ , the existence of the following set of  $k-1$  conditions is necessary and sufficient for the solvability of Eq. (9).

$$\begin{aligned} \tilde{\theta}_{m+k} &\notin [\beta_{m+1}^L, \beta_{m+1}^R] \\ \arg[\phi_{m+1}^{-1}(\tilde{\theta}_{m+k})] &\notin [\beta_{m+2}^L, \beta_{m+2}^R] \\ &\vdots \\ \arg[\phi_{m+k-2}^{-1} \circ \dots \circ \phi_{m+1}^{-1}(\tilde{\theta}_{m+k})] &\notin [\beta_{m+k-1}^L, \beta_{m+k-1}^R]. \end{aligned} \quad (\text{A3})$$

Two similar sets of  $k-1$  conditions each are obtained by substituting  $\arg[\tilde{\omega}_{m+k}^{R,L}]$  instead of  $\tilde{\theta}_{m+k}$  on the LHS of (A3), and their existence is necessary and sufficient for the solvability of Eq. (A2).

A failure of any of this conditions means that the  $k$ -th particle is overlapping at least one of the previous  $k-1$  particles. It is clear that if the two edge points of the particle are on the boundary of the  $m$ -particles cluster, so must be its tip (except very rare fill-up events [8] that we can safely neglect here). Therefore the existence of the last two sets of  $k-1$  conditions each is sufficient for the existence of the  $k-1$  conditions (A3).

## 2. Growth algorithms for $\mathcal{C} < 1$

The algorithm for growing one layer of  $p$  particles on the cluster made up of  $m$  particles (given  $\Phi^{(m)}$ ) is defined as follows:

1. Choose a series  $\{\tilde{\theta}_{m+k}\}_{k=1}^p$  uniformly distributed on the interval  $[0, 2\pi]$ .

2. Define  $\theta_{m+1} = \tilde{\theta}_{m+1}$ .
3. Calculate  $\lambda_{m+1}$  from Eq. (6), using the derivative of  $\Phi^{(m)}$  at the point  $e^{i\tilde{\theta}_{m+1}}$ .
4. Calculate  $\beta_{m+1}^{R,L}$  from Eq. (A1) and store them.
5. Let  $\mathcal{C}_1 = |\beta_{m+1}^R - \beta_{m+1}^L|/(2\pi)$

For  $k > 1$ :

6. Calculate  $\lambda_{m+k}$  by the derivative of  $\Phi^{(m)}$  at the point  $e^{i\tilde{\theta}_{m+k}}$ , and find the appropriate branch points  $\tilde{\omega}_{m+k}^{R,L}$ .
7. Check the  $2(k-1)$  conditions, given in Eq. (A3) upon replacing  $\tilde{\theta}_{m+k}$  by  $\arg[\tilde{\omega}_{m+k}^{R,L}]$  on the LHS of Eq. (A3). If any of them is violated (which means that the  $k$ -th particle overlaps one of the former  $k-1$  particles in the layer), choose another  $\tilde{\theta}_{m+k}$  and repeat from stage 6.
8. Solve Eqs. (9) and (A2) to find  $\theta_{m+k}$ ,  $\beta_{m+k}^R$ ,  $\beta_{m+k}^L$ , and store them.
9. Let  $\mathcal{C}_k = \mathcal{C}_{k-1} + |\beta_{m+k}^R - \beta_{m+k}^L|/(2\pi)$
10. After a series of  $p$  ‘‘good’’ angles  $\{\theta_{m+k}\}_{k=1}^p$  was found, such that all the  $p(p-1)$  solvability conditions resulting from  $p$  iterations of Eq. (A3) are fulfilled, update the conformal map according to Eq. (8) and  $\mathcal{C} = \mathcal{C}_p$ .

In our simulation  $p$  is not constant, but is determined by the value of  $\mathcal{C}$  that we want to achieve in each layer.

## 3. A full coverage ( $\mathcal{C} = 1$ ) growth algorithm

To reach  $\mathcal{C} = 1$ , we construct recursively a series of consecutive angles  $\{\theta_j\}_{j=m+1}^{m+p}$  such that the left branch cut of the  $j$ th particle coincides with the right branch cut of the  $(j+1)$ th particle. This reads

$$\Phi^{(j+1)}(\omega_{j+1}^R) = \Phi^{(j)}(\omega_j^L), \quad (\text{A4})$$

or

$$\beta_{j+1}^R = \arg[\phi_{j+1}(\omega_{j+1}^R)] = \arg[\omega_j^L]. \quad (\text{A5})$$

Given a pair  $(\theta_j, \lambda_j)$  (and hence  $\omega_j^{L,R}$  and  $\beta_j^{L,R}$ ) we have to choose  $\theta_{j+1}$  such that the value of  $\beta_{j+1}^R$  which is determined by  $\theta_{j+1}$  and the value of  $\lambda_{j+1}$  computed at  $\tilde{\theta}_{j+1}$  coincides with the previously computed  $\arg[\omega_j^L]$ . Numerically this is obtained as follows. We start with  $\theta_{j+1}$  far enough from  $\theta_j$ . Then, using Eqs.(6),(9),(A1), we calculate the appropriate values of  $\tilde{\theta}_{j+1}$ ,  $\lambda_{j+1}$  and  $\beta_{j+1}^R$ . This process is repeated until a value of  $\theta_{j+1}$  is found such that  $0 \leq \beta_{j+1}^R - \arg[\omega_j^L] \leq 0.01\sqrt{\lambda_j}$ . We proceed until the whole circle is covered.

## APPENDIX B: IMPOSING SYMMETRIES ON THE ITERATION SCHEME

In this appendix we explain how to use iterations of conformal maps to describe growth in geometries less symmetric than the radial. In addition we show how to preserve symmetries of the continuous Laplacian dynamics along the iterations. The basic idea will be demonstrated through the important example of growth in channel geometry, and straightforwardly employed to growth from initial conditions with reflection symmetry or  $n$ -fold symmetry in radial geometry.

### 1. Growth in a channel

The simplest symmetry that is preserved in the iterations scheme is  $2\pi$ -periodicity. Clearly,  $\phi_{\theta,\lambda}(e^{i\zeta}) = \phi_{\theta,\lambda}(e^{i(2\pi+\zeta)})$ . Therefore, if the initial conditions (i.e.  $\Phi^{(0)}$ ) have the property

$$\Phi^{(0)}(e^{i(2\pi+\theta)}) = \Phi^{(0)}(e^{i\theta}) + L \quad (\text{B1})$$

where  $L$  is the channel width, then  $\Phi^{(n)}$  will have this property for any  $n > 0$ . The simplest  $\Phi^{(0)}$  that has the periodicity property is of course  $\Phi^{(0)}(\omega) = \frac{2}{\pi} \log(\omega)$  ( $L = 1$ ) which describes a growth starting from a flat curve. Notice that the boundary conditions of the Laplacian field  $\nabla P = \frac{\Phi^{(n)'}}{|\Phi^{(n)}|}$  at infinity will be automatically changed from  $\nabla P \sim \frac{r}{r^2}$  to  $\nabla P \sim \text{const } \hat{x}$ .

Suppose now that we want to describe a growth in a channel with no-flow boundary conditions at the walls. This means that the Laplace problem has to be solved at each stage with the extra boundary conditions that the two walls  $y = 0$  and  $y = L$  are streamlines of the scalar field  $P$  (i.e.  $\frac{\partial P}{\partial y}|_{y=0,L} = 0$ ). Pre-images of streamlines of  $P$  in the physical plane are rays ( $\arg(\omega) = \text{const}$ ) in the mathematical plane. Therefore, imposing no-flow boundary conditions at the walls amounts to demanding that the two rays  $\arg(\omega) = \pm\epsilon$  ( $\epsilon \rightarrow 0$ ) are mapped under  $\Phi^{(n)}$  to the walls  $y = 0$  and  $y = L$  respectively, for every  $n$ .

Clearly, the elementary map  $\phi_{\theta,\lambda}(\omega)$  does not have this property. Except for  $\theta = 0, \pi$  the ray  $\arg(\omega) = 0$  is mapped to a curved line in the  $z$ -plane. Therefore, the appropriate boundary conditions at the walls are not respected by the iteration process.

We can overcome this difficulty in an analogous way to the image method used in electrostatics. Given initial conditions defined by some  $\tilde{\Phi}^{(0)}$  we construct our  $\Phi^{(0)}$  by:

$$\begin{aligned} \Phi^{(0)}(\omega) &= \tilde{\Phi}^{(0)}(2\omega) \quad \arg[\omega] \leq \pi \\ \Phi^{(0)}(\omega) &= \tilde{\Phi}^{(0)}(2\pi - \omega) + L \quad \arg[\omega] \geq \pi \end{aligned} \quad (\text{B2})$$

Under  $\Phi^{(0)}$  each half of the unit circle is mapped to another copy of the original interface with reflection symmetry around the real axis ( $\arg[\omega] = 0, \pi$ ). The pre-image

of the two walls  $y = 0$  and  $y = L$  under  $\Phi^{(0)^{-1}}$  are the rays  $\arg(\omega) = 0^+$  and  $\arg(\omega) = \pi$  (or  $\arg(\omega) = 0^-$  and  $\arg(\omega) = \pi$ ) respectively.

Now we construct an elementary conformal function that maps the rays  $\arg(\omega) = 0, \pi$  onto themselves. This can be achieved by choosing the elementary map to be

$$\phi_{\theta,\lambda} \circ \phi_{\bar{\theta},\lambda}(\omega), \quad (\text{B3})$$

such that the image of the unit circle will have the real line as a symmetry axis. This is shown schematically in Fig.12.

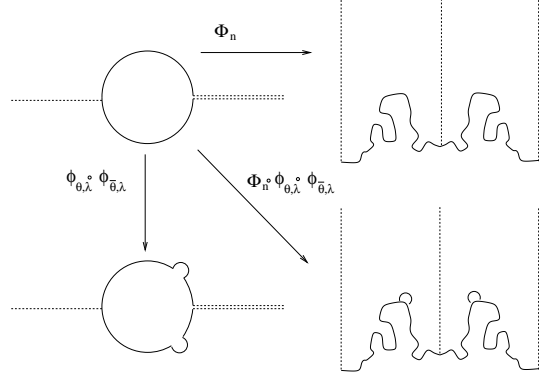


FIG. 12. Iterative conformal function that maps at each stage  $n$  the unit circle and the real axis in the mathematical plane to the evolving interface and the channel walls in the physical plane, respectively. The two rays  $\arg[\omega] = 0, \pi$  are mapped under  $\phi_{\theta,\lambda} \circ \phi_{\bar{\theta},\lambda}$  to themselves, and under the operation of  $\Phi^{(0)}$  to the walls  $y = 0, L$ .

Since the rays  $\arg(\omega) = 0, \pi$  are mapped to the walls under  $\Phi^{(0)}$  they will be mapped to the walls under  $\Phi^{(n)}$  defined by

$$\Phi^{(n)}(\omega) = \Phi^{(0)} \circ \phi_{\theta_1,\lambda_1} \circ \phi_{\bar{\theta}_1,\lambda_1} \circ \dots \circ \phi_{\theta_n,\lambda_n} \circ \phi_{\bar{\theta}_n,\lambda_n}(\omega) \quad (\text{B4})$$

Naively, one may think that  $\bar{\theta} = -\theta$ . However, constructing the symmetric map as a composition of two non-symmetric maps leads to some complication. In order to have a symmetric image of the unit circle, one would like to have the second bump in the image of the unit circle to be located exactly symmetrically to the first bump:

$$\phi_{\theta,\lambda}(e^{i\bar{\theta}}) = e^{-i\theta}. \quad (\text{B5})$$

Eq. (B5) implies choosing  $\bar{\theta}$  according to

$$\bar{\theta} = \arg[\phi_{\theta,\lambda}^{-1}(e^{-i\theta})]. \quad (\text{B6})$$

The difference  $|\bar{\theta} - (-\theta)|$  becomes smaller with  $\lambda$ , and is zero at the points  $\theta = 0, \pi, \pm\pi/2$  for every value of  $\lambda$ .

## 2. Preserving symmetries of the Laplacian dynamics

The simple technique that was developed in the previous subsection can be generalized for cases in which a symmetry of the Shraiman-Bensimon Eq. (17) is known for specific initial conditions and we want to preserve it upon using iterations of conformal maps.

### a. reflection symmetry in radial geometry

Suppose that the initial interface has a reflection symmetry with respect to some axis. Without loss of generality we can take the symmetry axis to be the  $x$ -axis, which is the image under  $\Phi^{(0)}$  of the real axis in the mathematical plane. Then:

$$\Phi^{(0)}(\omega^*) = [\Phi^{(0)}(\omega)]^* \quad (\text{B7})$$

It is easy to prove that this symmetry will be preserved under the Shraiman-Bensimon dynamics.

In order to respect this symmetry in our iterative scheme we use again the elementary map (B3) which has reflection symmetry with respect to the real axis. Thus,  $\Phi^{(n)}(\omega)$ , defined by Eq. (B4) with  $\Phi^{(0)}$  that has the property (B7) will preserve reflection symmetry.

### b. $n$ -fold symmetry in radial geometry

The Shraiman-Bensimon Equations preserve also  $n$ -fold symmetry. Therefore, if the initial interface, defined by  $\Phi^{(0)}$  has this symmetry, so should do  $\Phi^{(n)}$ . For simplicity let us consider 3-fold symmetry of the form:

$$\Phi^{(0)}(e^{\frac{2\pi i}{3}}\omega) = e^{\frac{2\pi i}{3}}\Phi^{(0)}(\omega). \quad (\text{B8})$$

In order for this symmetry to be preserved, the elementary map must be 3-fold symmetric as well. Following the discussion in the first part of this appendix this can be achieved by choosing the elementary map to be

$$\phi_{\theta,\lambda} \circ \phi_{\bar{\theta},\lambda} \circ \phi_{\hat{\theta},\lambda}(\omega), \quad (\text{B9})$$

where

$$\begin{aligned} \bar{\theta} &= \arg[\phi_{\theta,\lambda}^{-1}(e^{\frac{2\pi i}{3}}\theta)] \\ \hat{\theta} &= \arg[\phi_{\bar{\theta},\lambda}^{-1} \circ \phi_{\theta,\lambda}^{-1}(e^{\frac{4\pi i}{3}}\theta)]. \end{aligned} \quad (\text{B10})$$

The evolution equation for  $\Phi^{(n)}$  now reads

$$\begin{aligned} \Phi^{(n)}(\omega) &= \Phi^{(0)} \circ \phi_{\theta_1,\lambda_1} \circ \phi_{\bar{\theta}_1,\lambda_1} \circ \phi_{\hat{\theta}_1,\lambda_1} \circ \dots \circ \\ &\circ \dots \circ \phi_{\theta_n,\lambda_n} \circ \phi_{\bar{\theta}_n,\lambda_n} \circ \phi_{\hat{\theta}_n,\lambda_n}(\omega). \end{aligned} \quad (\text{B11})$$

The extension to higher symmetries is straightforward.

## APPENDIX C: CONSTRUCTING AN OUTLINE FROM BRANCH POINTS

The common method [8] to produce the outline of  $n$ -particles cluster constructed by the iterated conformal map technique is to sample the unit circle at  $K$  angles  $\{\theta_k\}_{k=1}^K$  and to plot their images under the map  $\{\Phi^{(n)}(e^{i\theta_k})\}_{k=1}^K$ . This simple method is problematic since a uniform series  $\{\theta_k\}$  will sample the tips much more than the fjords, and thus in order to have a reasonable image of the fjords (which are the major part of the fractal cluster), a huge number  $K \gg n$  has to be used. Since calculation of each image point  $\Phi^{(n)}(e^{i\theta_k})$  calls for  $O(n^2)$  operations, this turns out to be a very inefficient method.

Here we propose an algorithm of  $O(n^2)$  complexity to produce an exhaustive real-space image of the whole cluster. The key idea is to focus attention on the edge points of the particles, which are the images of the branch points of the map  $\Phi^{(n)}$  on the unit circle. Each growing particle adds on two new branch points to the evolving map and may remove some old ones due to overlaps (see discussion in Appendix A). Therefore, the number of ‘‘exposed’’ branch points of  $\Phi^{(n)}$  is bounded by  $2n$ . Let us denote these points  $\{\omega_k^{R,L}\}_{k=1}^n$ . An exposed branch point  $\omega_k^{R,L}$  was added to the conformal map by the  $k$ -th growing particle, and since this particle was not overlapped by any of the next  $n - k$  particles it remains as a branch point of the map  $\Phi^{(n)}$ . Nevertheless, the reparametrization of the unit circle induced by the following  $n - k$  iterations changes the pre-image of each branch point from  $\omega_k^{R,L}$  to  $\omega_{k,n}^{R,L}$ . The connection between  $\omega_k^{R,L}$  and  $\omega_{k,n}^{R,L}$  is given, similarly to Eq. (7) by:

$$\Phi^{(k)}(\omega_k^{R,L}) = \Phi^{(n)}(\omega_{k,n}^{R,L}), \quad (\text{C1})$$

which can be simplified to

$$\omega_{k,n}^{R,L} = \phi_{\theta_{n-1},\lambda_{n-1}}^{-1} \circ \dots \circ \phi_{\theta_{k+1},\lambda_{k+1}}^{-1}(\omega_k^{R,L}). \quad (\text{C2})$$

The solvability of Eq. (C2) determines whether the appropriate edge point of the  $k$ -th particle remains exposed under the addition of the next  $n - k$  particles. Checking the solvability conditions and calculating the reparametrized branch points  $\omega_{k,n}^{R,L}$  from Eq. (C2) is performed in the same way as in Appendix A, and it consists of  $O([k - n]^2)$  operations. The total complexity of the algorithm is therefore  $O(n^2)$ .

- 
- [1] L. Paterson, Phys. Rev. Lett. **52**, 1621 (1984); L.M. Sander, Nature **322**, 789 (1986); J. Nittmann and H.E. Stanley, Nature **321**, 663 (1986); H.E. Stanley, in ‘‘Fractals and disordered systems’’, A. Bunde and S. Havlin (Eds.), Springer-Verlag (1991).

- [2] P.G. Saffman and G.I. Taylor, Proc. Roy. Soc. London Series A, **245**,312 (1958).
- [3] B. Shraiman and D. Bensimon, Phys.Rev. **A30**, 2840 (1984); S.D. Howison, J. Fluid Mech. **167**, 439 (1986).
- [4] T.A. Witten and L.M. Sander, Phys. Rev. Lett, **47**, 1400 (1981).
- [5] D. Bensimon, L.P. Kadanoff, S. Liang, B.I. Shraiman and C. Tang, Rev. Mod. Phys. **58**, 977 (1986); S. Tanveer, Phil. Trans. R. Soc. Lond. **A343**, 155 (1993) and references therein.
- [6] F. Barra, B. Davidovitch, A. Leverman and I. Procaccia arXiv:cond-mat/0103126.
- [7] M.B. Hastings and L.S. Levitov, Physica D **116**, 244 (1998).
- [8] B. Davidovitch, H.G.E. Hentschel, Z. Olami, I.Procaccia, L.M. Sander, and E. Somfai, Phys. Rev. E, **59** 1368 (1999).
- [9] B. Davidovitch, M.J. Feigenbaum, H.G.E. Hentschel and I. Procaccia, Phys. Rev. E **62**, 1706 (2000).
- [10] M. G. Stepanov and L. S. Levitov arXiv:cond-mat/0005456
- [11] B. Davidovitch and I. Procaccia, Phys. Rev. Lett., **85** 3608-3611 (2000).
- [12] B. Davidovitch, A. Levermann, I. Procaccia, Phys. Rev. E, **62** R5919.
- [13] E. Ben-Jacob, R. Godbey, N.D. Goldenfeld, J. Koplik, H. Levine, T. Mueller and L.M. Sander, Phys. Rev. Lett. **55**, 1315 (1985); J.D. Chen, Exp. Fluids **5**, 363 (1987); A. Arneódo, Y. Couder, G. Grasseau, V. Hakim, M. Rabaud, Phys. Rev. Lett. **63**, 984 (1989).
- [14] W-S Dai, L.P. Kadanoff and S-M Zhou, Phys. Rev. A **43**, 6672 (1991).
- [15] T.C. Halsey, Phys. Rev. Lett. **72**, 1228 (1994).